1.1 Stripline Kicker Design for Beam Extraction from the CLIC Damping Rings

C. Belver-Aguilar, A. Faus-Golfe,
Instituto de Física Corpuscular, Valencia (IFIC)
F. Toral,
Centro de Investigaciones Energéticas, Medioambientales y Tecnológicas
(CIEMAT)
M.J. Barnes
European Organization for Nuclear Research (CERN)
Mail to: cbelver@ific.uv.es, afaus@ific.uv.es, fernando.toral@ciemat.es,
Mike.Barnes@cern.ch

1.1.1 Introduction

The injection and extraction systems of the CLIC PDRs and DRs consist of a FODO cell with kicker and septum magnets in the drift spaces to deflect the beam. The injection and extraction kickers are located at symmetric locations, after the dispersion suppressor and upstream of the super-conducting wigglers, to avoid damage from synchrotron radiation [1]. The main kicker parameters are shown in Table 1.

Table 1: Kicker specifications for the PDRs and DRs for electrons [2].

Kicker parameters	Symbol	PDRs 1/2 GHz	DRs 1/2 GHz
Deflection angle (mrad)	α	2.0	1.5
Aperture (mm)	a	40	20
Effective length (m)	L	3.4	1.7
Field rise and fall time (ns)		428/1000	560/1000
Pulse flat top (ns)		900/160	900/160
Flat top reproducibility		$\pm 1 \times 10^{-4}$	$\pm 1 \times 10^{-4}$
Injection stability		$\pm 2 \times 10^{-2}$	$\pm 2 \times 10^{-3}$
Extraction stability		$\pm 2 \times 10^{-3}$	$\pm 2 \times 10^{-4}$
Injection uniformity (%)		$\pm 0.1^{a}$	$\pm \pm 0.1^{a}$
Extraction uniformity (%)		$\pm 0.1^{a}$	$\pm 0.01^{b}$
Repetition rate (Hz)	f_{rep}	50	50
Vacuum (mbar)		10^{-10}	10^{-10}
Stripline voltage (kV)	V_k	± 17.0	± 12.5
Stripline current (A)	I_k	± 340	± 250
Longitudinal beam impedance (Ω/n) [3]	$Z_{\parallel}$	0.05	0.05
Transverse beam impedance (kΩ) [3]	$Z_{\perp}$	200	200

[a]over 3.5 mm radius
[b]over 1 mm radius

1.1.2   Stripline Kicker operation

A stripline-type kicker has been proposed for the extraction kicker of the CLIC DRs. It consists of two parallel electrodes housed in a conducting cylinder: each of the electrodes is driven by an equal but opposite polarity pulse. A 3D model of the stripline kicker prototype is shown in Fig. 1.
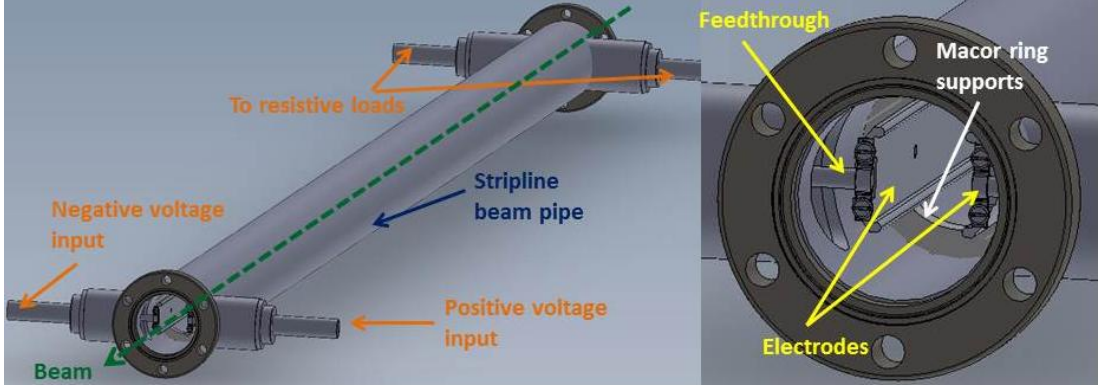
Figure 1: 3D model of a stripline kicker.

The stripline kicker operates as two coupled transmission lines with two operating modes: odd and even mode. When the electrodes are excited with equal magnitude but opposite polarity voltages, the current flow is in opposite directions in each stripline electrode and an electromagnetic field is created between the electrodes, giving a transverse kick to the beam: this is the odd mode. When unkicked circulating beam passes through the aperture of the striplines, it induces image currents in the electrodes: the direction of current flow is the same in both electrodes - this is the even mode. The induced current generates an electromagnetic field, which gives a longitudinal kick to the beam and can produce beam instabilities.

1.1.3   Design of the stripline geometry

1.1.3.1   *Characteristic impedance and field homogeneity optimization*

The electrode cross section was selected by studying several shapes for the striplines and optimizing each shape to achieve 50 Ω even mode characteristic impedance, in order to minimize impedance mismatches seen by the beam, and ±0.01% field inhomogeneity over a circle of 1 mm radius at the centre of the aperture. The odd mode impedance of each optimized shape was also calculated. Ensuring that the odd mode characteristic impedance of each electrode is close to 50 Ω will avoid large mismatches to the characteristic impedance of feedthroughs, coaxial cables and the inductive adder.

The most common electrode shapes for striplines, used in injection/extraction kickers, are flat and curved electrodes [4-6]. Flat electrodes show good field homogeneity, whereas curved electrodes may allow for a better impedance matching between the two operation modes, but with poorer field homogeneity. Hence a new geometry was proposed: the half-moon electrode. This new electrode shape allows for both features, i.e. good field homogeneity and suitable impedance matching. The geometric parameters used to optimize the shape of the electrodes are shown in Fig. 2.
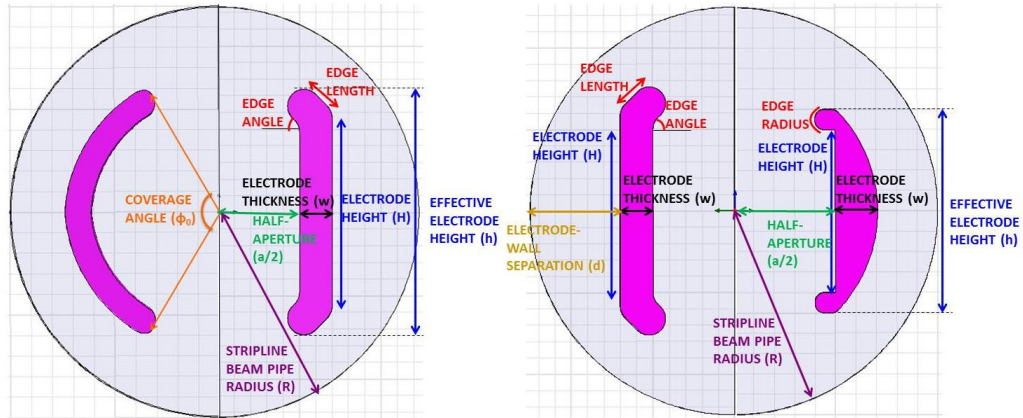
Figure 2: Schematic of the geometric parameters, for a curved and a flat electrode (left), and t for a flat and a half-moon electrode (right).

Only with flat electrodes and half-moon electrodes it is possible to achieve the required field homogeneity. For flat electrodes with 50 Ω even mode characteristic impedance, an odd mode characteristic impedance of 36.8 Ω was achieved with a stripline beam pipe radius of 25 mm. For the half-moon electrodes the odd mode characteristic impedance is 40.9 Ω. The higher odd mode impedance for the half-moon electrodes is due to the fact that the distance between the electrode and the stripline beam pipe, optimized for field homogeneity, is smaller than for the flat electrodes, which leads to a closer values for the odd mode and even mode characteristic impedances. Therefore, flat and half-moon electrodes have been studied further and, in the following sections, the features of both electrode shapes are compared, which allows the final geometric design of the striplines to be chosen.

1.1.3.2   *Power transmission through the striplines*

The coaxial feedthroughs have 50 Ω characteristic impedance outside of the beam pipe, however, the characteristic impedance of the connection to the electrode is not 50Ω. Furthermore, during the kicker operation, the electrode (odd mode) characteristic impedance is lower than 50 Ω. These impedance mismatches will result in power being reflected. HFSS has been used to study the S_{11} parameter, and the results are shown in Fig. 3.
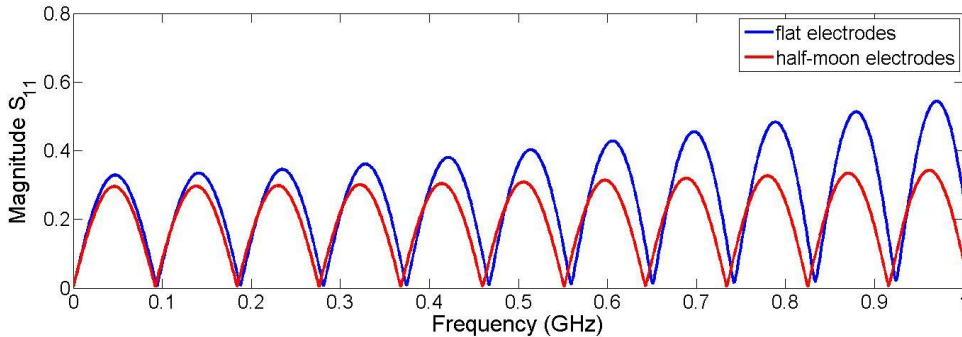
Figure 3: S_{11} for flat electrodes (blue) and half-moon electrodes (red), for a frequency range from DC to 1 GHz.

The peaks of S_{11} increase with frequency, with more impact for the flat electrode. The shape of the curves depends on the coaxial feedthrough to electrode transition, and

the frequency difference between peaks is related to the electrode length as $\Delta f = c/2L \approx 90$ MHz. The half-moon electrode has a reflection magnitude below 0.35 over the whole frequency range analyzed (up to 1 GHz), whereas the flat electrode shape has a reflection parameter consistently below 0.35 only up to approximately 350 MHz.

1.1.3.3 *Settling time*

Impedance mismatches create reflections and thus ripple of the driving pulse. The time for the ripple to reduce within specification (± 0.02 %) is called the settling time: settling time is measured from the end of the rise time. An inductive adder will be used to power each stripline electrode [7]. From the inductive adder point of view, settling time should be as low as possible; settling time increases the required pulse width, thus increasing power dissipation and cross-sectional area of magnetic material. Hence the aim is to limit settling time (T_s) such that is no more than 100 ns.

Figure 4 shows the predicted settling time versus odd mode characteristic impedance of the electrodes, for different 0% to 100% rise times of the output pulse of the inductive adder. For flat electrodes, an odd mode characteristic impedance of 36.8 Ω results in a settling time of 113 ns for a rise-time of the output pulse, from the inductive adder, of 100 ns. For the same rise-time, a settling time of 78 ns will result when the odd mode characteristic impedance is 40.9 Ω, which is the case for the half-moon electrodes. Therefore, half-moon electrodes allow for a reduced settling time, which is beneficial for the design of the inductive adder.
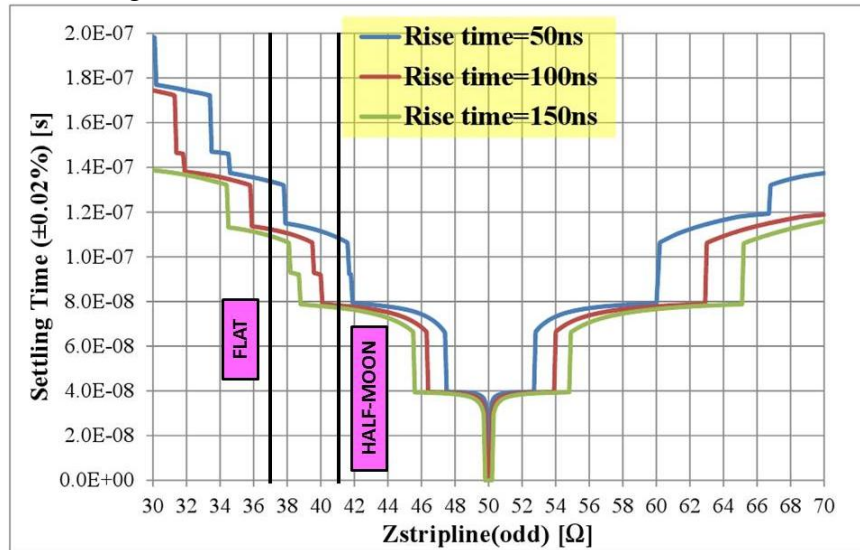
Figure 4: Settling time of the stripline voltage pulse as a function of stripline impedance for different 0% to 100% rise times of the output pulse of the inductive adder. The inductive adder, transmission line and terminating resistor impedances are 50 Ω.

1.1.3.4 *Beam coupling impedance*

The permissible beam coupling impedances, per kicker system, are assumed to be 5% of the longitudinal impedance allowance, i.e. $0.05 \Omega/n$, and 2% of the transverse impedance allowance, i.e. 200 kΩ/m [3].

At low frequencies, analytical equations for the longitudinal and transverse coupling impedance, $Z_{\parallel}$ and $Z_{\perp}$, respectively, for untapered stripline beam position monitors, are shown in [8]:

$$Z_{\parallel} = 2Z_{even}\left(\frac{\phi_0}{2\pi}\right)^2\left[2\sin^2\left(\frac{\omega L}{c}\right) - i\sin\left(\frac{2\omega L}{c}\right)\right] \qquad (1)$$

$$Z_{\perp} = \left[\frac{Z_{\parallel}}{\omega}\right]_{pair}\left[\frac{c}{R^2}\right]\left[\frac{4}{\phi_0}\right]^2\left[\sin^2\left(\frac{\phi_0}{2}\right)\right] \qquad (2)$$

where ϕ_0 is the coverage angle of a single electrode, ω is the angular frequency, L the striplines length and R the stripline beam-pipe radius. For the proposed striplines of approximately 1.7 m length, the even mode characteristic impedance (Z_{even}) is 50 Ω and the coverage angle ϕ_0, for each stripline, is 2.0 and 1.8 radians, for a flat electrode and a half-moon electrode, respectively.

By using the code CST Particle Studio (PS), the beam coupling impedance has been studied and compared with the analytical equtions. Results for untapered striplines are shown in Fig. 5 and Fig. 6, for longitudinal and transverse beam coupling impedance, respectively. The results show good agreement between analytical calculations and predictions from simulations. The magnitude of the low frequency peak for the longitudinal beam coupling impedance is lower in the case of half-moon electrodes. The reason for this can be understood from Eq. 1: longitudinal beam coupling impedance is proportional to the square of the coverage angle. Transverse beam coupling impedance is initially lower in the case of flat electrodes, since the stripline beam pipe radius is larger in this case (Eq. 2).
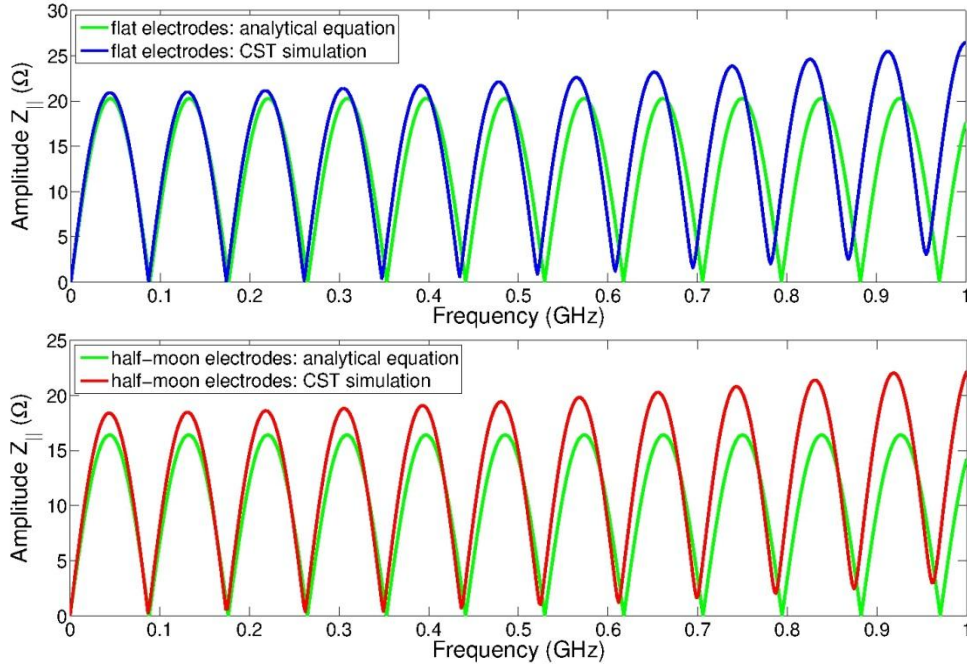
Figure 5: Longitudinal beam coupling impedance results for untapered striplines from both Eq.1 (green) and CST PS simulations for flat electrodes (blue) and half-moon electrodes (red).
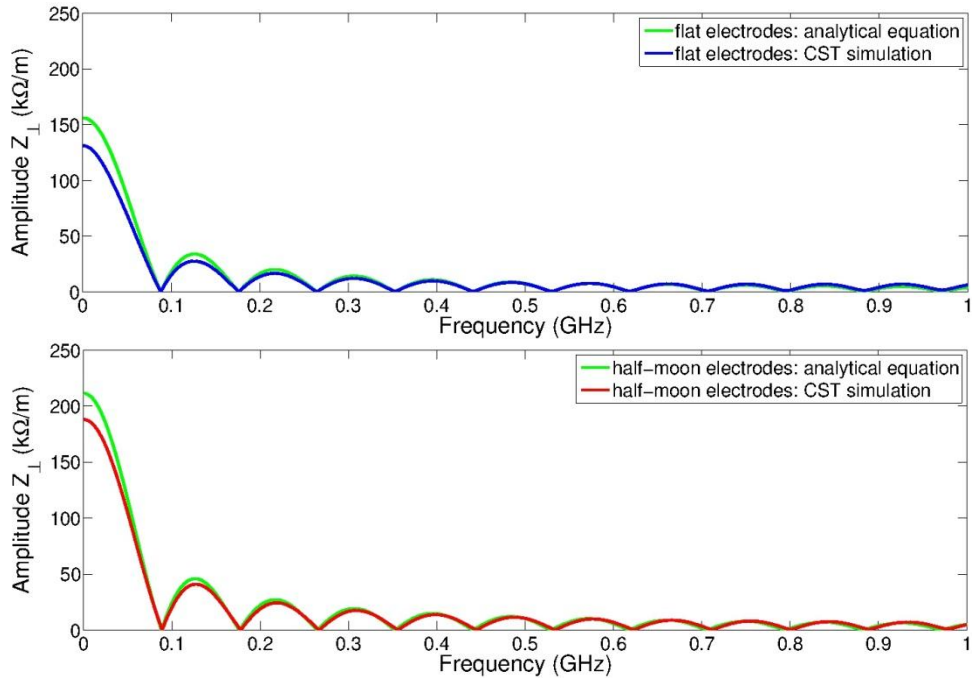
Figure 6: Transverse beam coupling impedance results for untapered striplines from both Eq. 2 (green) and CST PS simulations for flat electrodes (blue) and half-moon electrodes (red).

1.1.3.5 *Discussion and choices of the stripline geometry*

Studies of the cross-section of the striplines for the extraction kicker of the CLIC DRs have shown that for a 50 Ω even mode characteristic impedance of the striplines and the field homogeneity required, the half-moon electrode shape results in an odd mode characteristic impedance closer to 50 Ω than the flat electrodes. Furthermore, the reflection coefficient predicted looking into the input port, with 50 Ω on each output port, shows that the transmission is slightly better in the case of half-moon electrodes (Fig. 3), hence the settling time (Fig. 4) is reduced. Finally, simulations of beam coupling impedance show that the longitudinal beam coupling impedance is lower for the half-moon electrode (Fig. 5), whereas the flat electrode shape is better from the transverse beam coupling impedance point of view (Fig. 6).

Overall, the half-moon electrodes are considered as the best choice for the cross-section of the striplines for the extraction kicker of the CLIC DRs.

1.1.4 Stripline Kicker Components

1.1.4.1 *Study and optimization of the electrode supports*

The electrodes have a total length of 1.639 m and, ideally, must be perfectly aligned along their entire length. In order to ensure the alignment, the electrodes are fixed outside the aperture by using four equally-spaced Macor rings, of 10 mm length each. Once the electrodes are aligned and fixed to the Macor rings, this assembly will be placed inside the stainless steel tube.
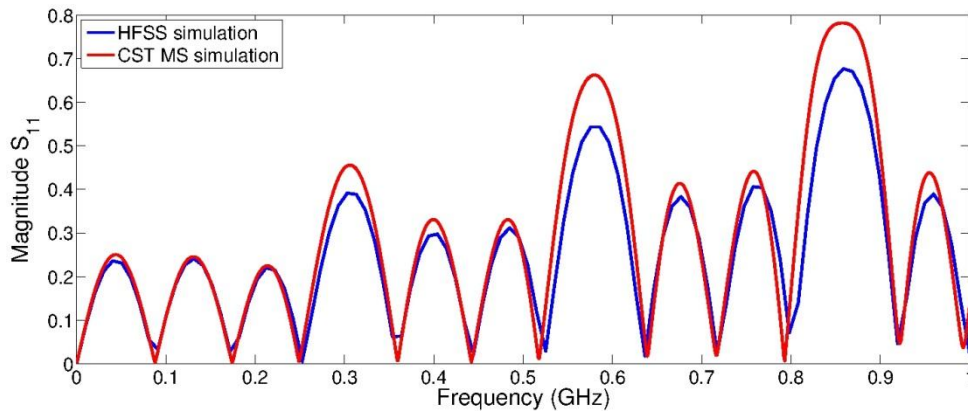
Figure 7: Magnitude of S_{11} predicted by HFSS and CST Microwave Studio (MS), for striplines with four equally-spaced Macor ring supports, and ideal 50 Ω feedthroughs.

Figure 7 shows that the Macor rings increase the magnitude of the reflection parameter S_{11}, starting from 300 MHz, of every third peak. The separation between these maxima corresponds to the distance, there and back, between the equally-spaced Macor rings (510 mm). However, the frequency content of the driving pulse from the inductive adder will only extend up to approximately $f = 0.35/T_r \approx 7$ MHz, where the pulse rise time considered is $T_r = 50$ ns. Thus, since the Macor rings mainly affect the S_{11} above 300 MHz, they are not expected to significantly influence the ripple of the driving pulse.
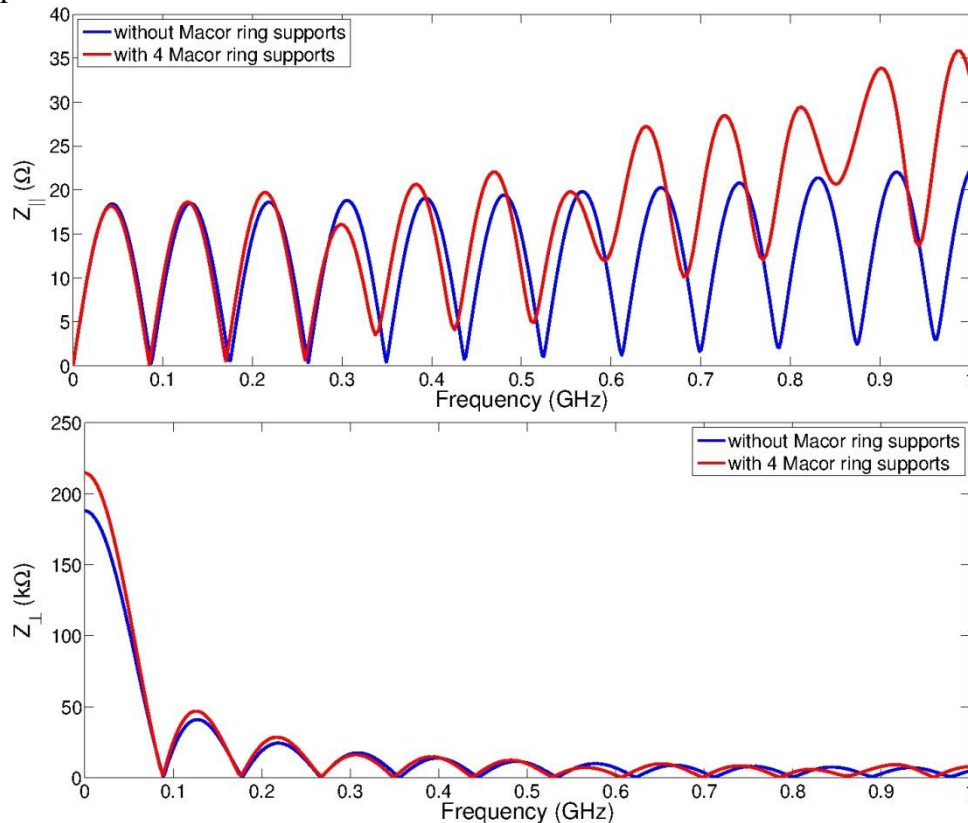
Figure 8: Longitudinal (top) and transverse (bottom) beam coupling impedance for striplines with and without Macor rings, simulated with CST PS, for ideal 50 Ω feedthroughs.

From the beam coupling impedance point of view, the presence of the Macor rings increases the energy lost by the beam particles when passing through the aperture. Hence there is an increase of the longitudinal beam coupling impedance above ≈330MHz (Fig. 8, top), whereas the transverse beam coupling impedance (Fig. 8, bottom) is not significantly affected because the Macor rings do not change the cross-section of the striplines.

1.1.4.2 *Feedthroughs study and optimization*

To study the effects of the feedthroughs upon the power reflected, a model with ideal coaxial feedthroughs was first used. Once we chose the Kyocera 15kV-F-UHV feedthroughs [9], they were simulated and results are shown in Fig. 9.
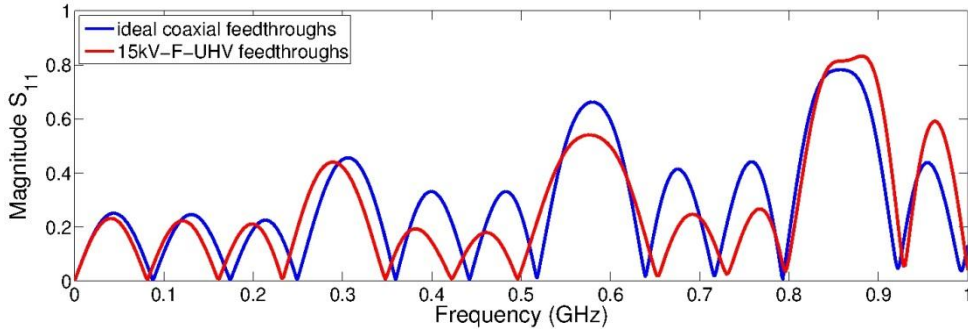
Figure 9: Predicted magnitude of S_{11} for striplines with ideal coaxial feedthroughs and with Kyocera 15kV-F-UHV feedthroughs.

Figure 9 shows that up to ≈800 MHz the magnitude of the S_{11} parameter is generally lower with the commercial feedthroughs than with the ideal feedthroughs. This is due to the impedance of the connection between the feedthrough and the striplines being lower than 50 Ω up to 800 MHz. Furthermore, a frequency shift is observed in the maxima and minima pattern for the two models. This is due to the change in the dielectric from only vacuum for both the ideal coaxial feedthrough and the transition to the electrode, to Al_2O_3 for the Kyocera coaxial feedthrough and back to vacuum for the transition: the different dielectric constant results in a change in the velocity of the pulse signal, and therefore a frequency shift.

In addition, simulations of beam coupling impedance have been carried out: preliminary results from the model with the Kyocera feedthroughs do not show any difference compared to the model simulated using ideal 50 Ω feedthroughs. Changes in the beam coupling impedance could occur at high frequencies; however, it has not been possible to run CST PS simulations at higher frequencies than 5 GHz.

1.1.5 Conclusions

The electromagnetic design of the striplines, including a detailed study of the electrode supports and the feedthroughs, has been carried out. The stripline design provides the performance specified for the extraction kicker of the CLIC DRs: excellent field homogeneity, good power transmission and low broadband beam coupling impedance. A first prototype of the extraction stripline kicker for the CLIC DR has been manufactured by Trinos Vacuum Projects (Valencia, Spain), and will be tested with and without beam, as well as with and without the inductive adder, in the near future.

1.1.6 References

1. R. Apsimon, B. Balhan, M.J. Barnes, J. Borburgh, B. Goddard, Y. Papaphilippou, J. Uythoven, "Optics and protection of the injection and extraction regions of the CLIC damping rings", proceedings of the 4th International Particle Accelerator Conference (IPAC, 2013).
2. A multi-TeV linear collider based on CLIC technology: CLIC Conceptual Design Report (CDR, 2012).
3. G. Rumolo, private communication.
4. T. Naito, H. Hayano, M. Kuriki, N. Terunuma, J. Urakawa, "Development of a 3 ns rise and fall time strip-line kicker for the International Linear Collider", Nuclear Instruments and Methods in Physics Research A 571 (2007).
5. I. Rodríguez, "Calculation methodology and fabrication procedures for particle accelerator strip-line kickers: application to the CTF3 combiner ring extraction kicker and TL2 tail clippers", PhD thesis, Universidad Politécnica de Madrid (2009).
6. D. Alesini, S. Guiducci, F. Marcellini, P. Raimondi, "Design, test and operation of new tapered stripline injection kickers for the e^+e^- collider DAΦNE", Physical Review Special Topics −Accelerators and Beams, 13, 111002 (2010).
7. J. Holma, M.J. Barnes, S.J. Ovaska, "Modelling of parasitic inductances of a high precision inductive adder for CLIC", proceedings of the 4th International Particle Accelerator Conference (IPAC, 2013).
8. W. Chao, Handbook of Accelerator Physics and Engineering, 3rd Edition (2006).
9. http://global.kyocera.com